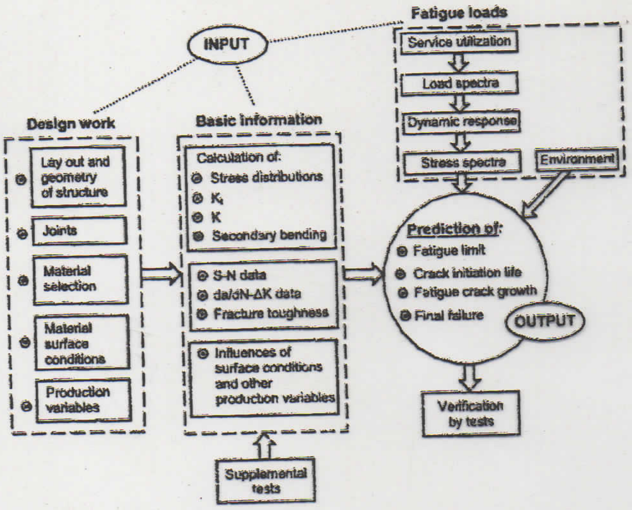

Fig. 1. Survey of the various aspects of fatigue of structures [11].

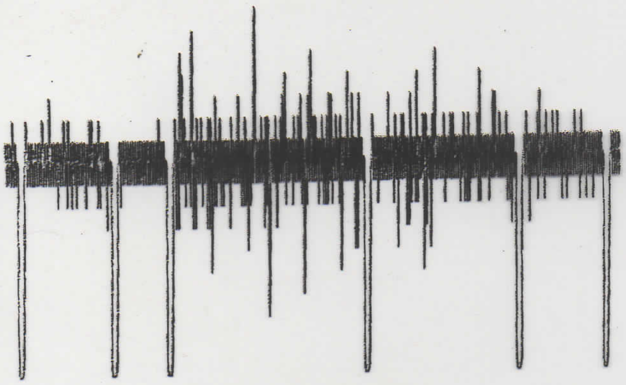

Fig. 17. Sample of a load history applied in flight-simulation fatigue tests. Five flights are shown with gust loads corresponding to different weather conditions.

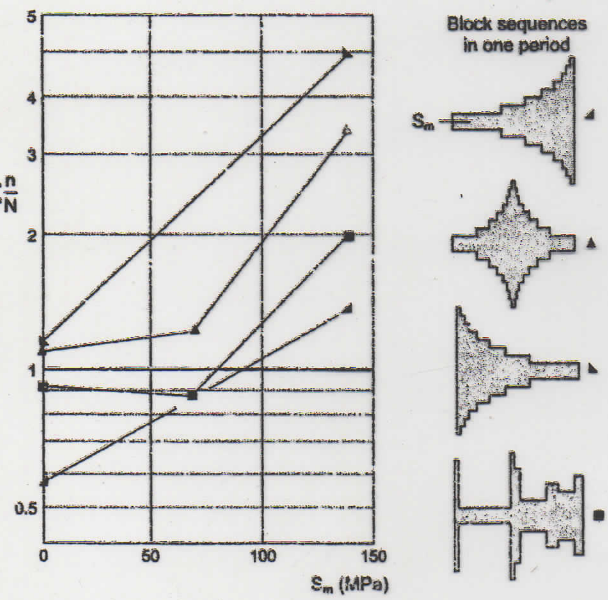

Fig. 14. The effect of overloads (OL) on fatigue crack growth in sheet specimens of the 2024-T3 Al-alloy [74].

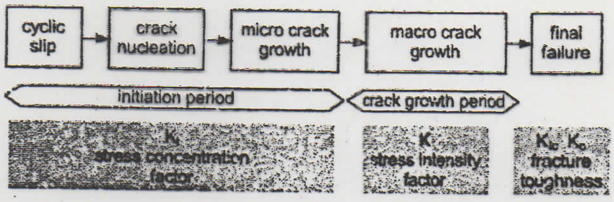

Fig. 6. Different phases of the fatigue life and relevant factors.

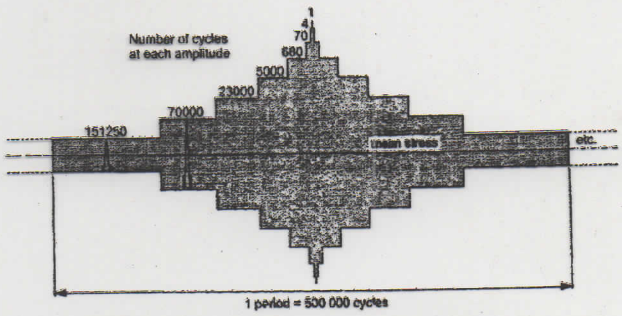

Fig. 18. Block-programme fatigue test introduced by Gassner [89]. CA-load cycles in each block. Blocks in a low-high-low sequence of the amplitude.

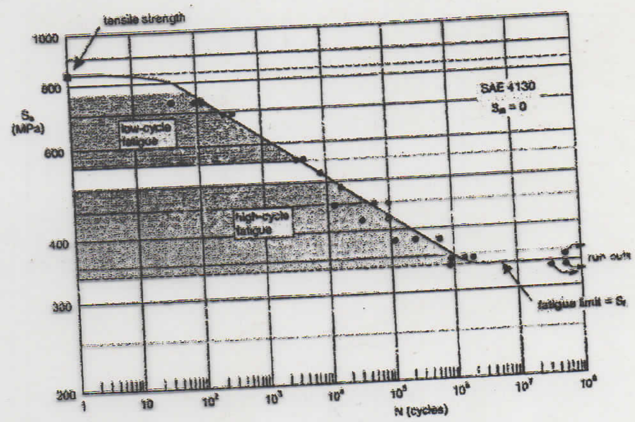

Fig. 11. Fatigue test results of unnotched specimens of a low alloy steel (NACA TN 2324, 1951). Regions of low-cycle and high-cycle fatigue.

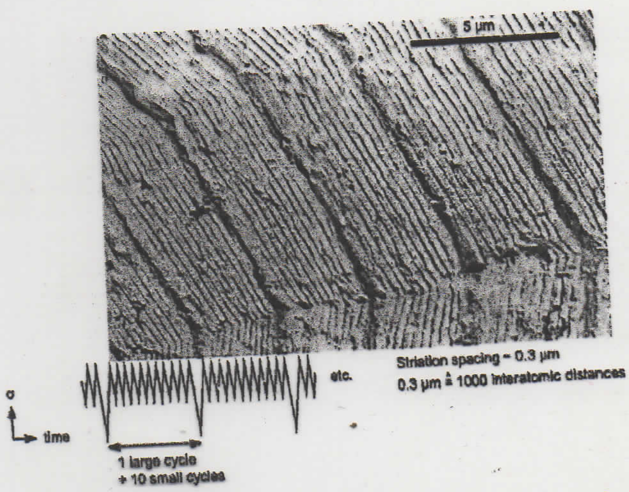

Fig. 3. Correspondence between striations and load cycles during fatigue crack growth in an Al-alloy specimen (picture Nat. Aerospace Lab., NLR, Amsterdam).

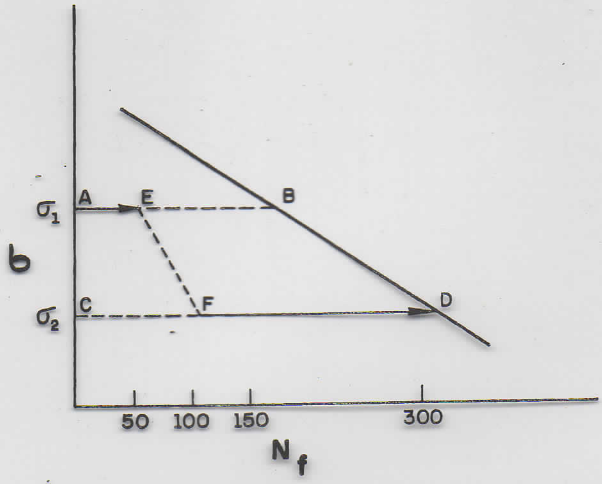

Figure 14.9 Damage accumulation, in a high-to-low loading sequence. (Adapted with permission from B. I. Sandor, *Fundamentals of Cyclic Stress and Strain* (Madison, WI: University of Wisconsin Press, 1972)

Figure 14.11 Well-developed maze structure, showing dislocation walls on {100} in Cu–Ni alloy fatigued to saturation. (From P. Charsley, *Mater. Sci. & Eng.*, 47 (1981) 181)

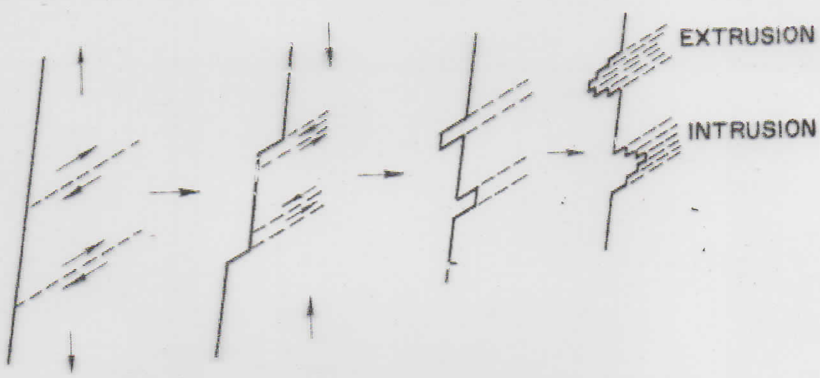

Figure 14.12 Fatigue crack nucleation at slip bands.

Figure 14.13 SEM of extrusions and intrusions in a copper sheet. (Courtesy of M. Judelwicz and B. Ilschner)

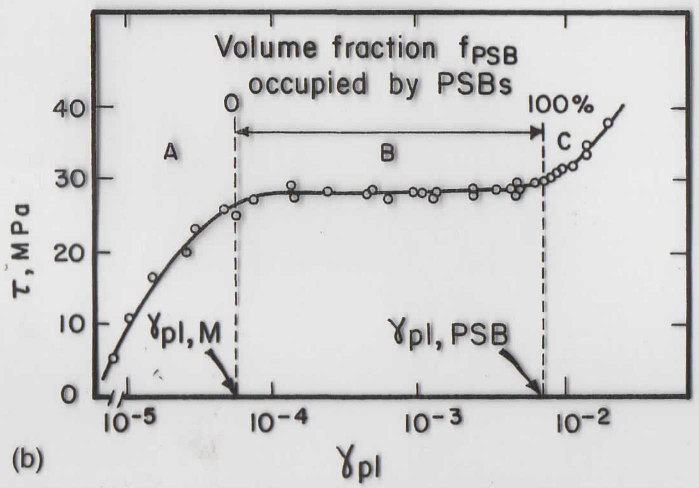

(b)

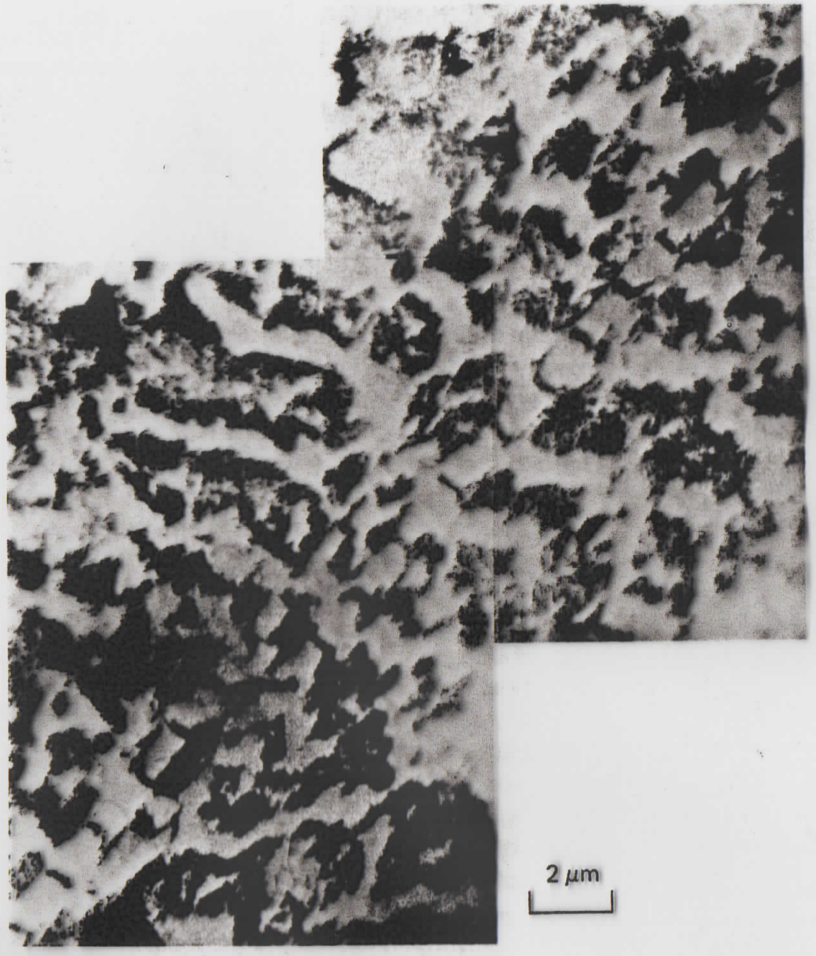

(a)

Figure 14.10 (a) Persistent slip bands in vein structure. Polycrystalline copper fatigued at a total strain amplitude of 6.4×10^{-4} for 3×10^5 cycles. Fatiguing carried out in reverse bending at room temperature and at a frequency of 17 Hz. The thin foil was taken 73 μm below the surface. (Courtesy of J. R. Weertman and H. Shirai) (b) Cyclic stress–strain curve for a single crystal of copper oriented for single slip (After H. Mughrabi, *Mater. Sci. & Eng.*, 33 (1978) 207)

Figure 14.11 Well-developed maze structure, showing dislocation walls on {100} in Cu–Ni alloy fatigued to saturation. (From P. Charsley, *Mater. Sci. & Eng.*, 47 (1981) 181)

Figure 14.13 SEM of extrusions and intrusions in a copper sheet. (Courtesy of M. Judelwicz and B. Ilschner)

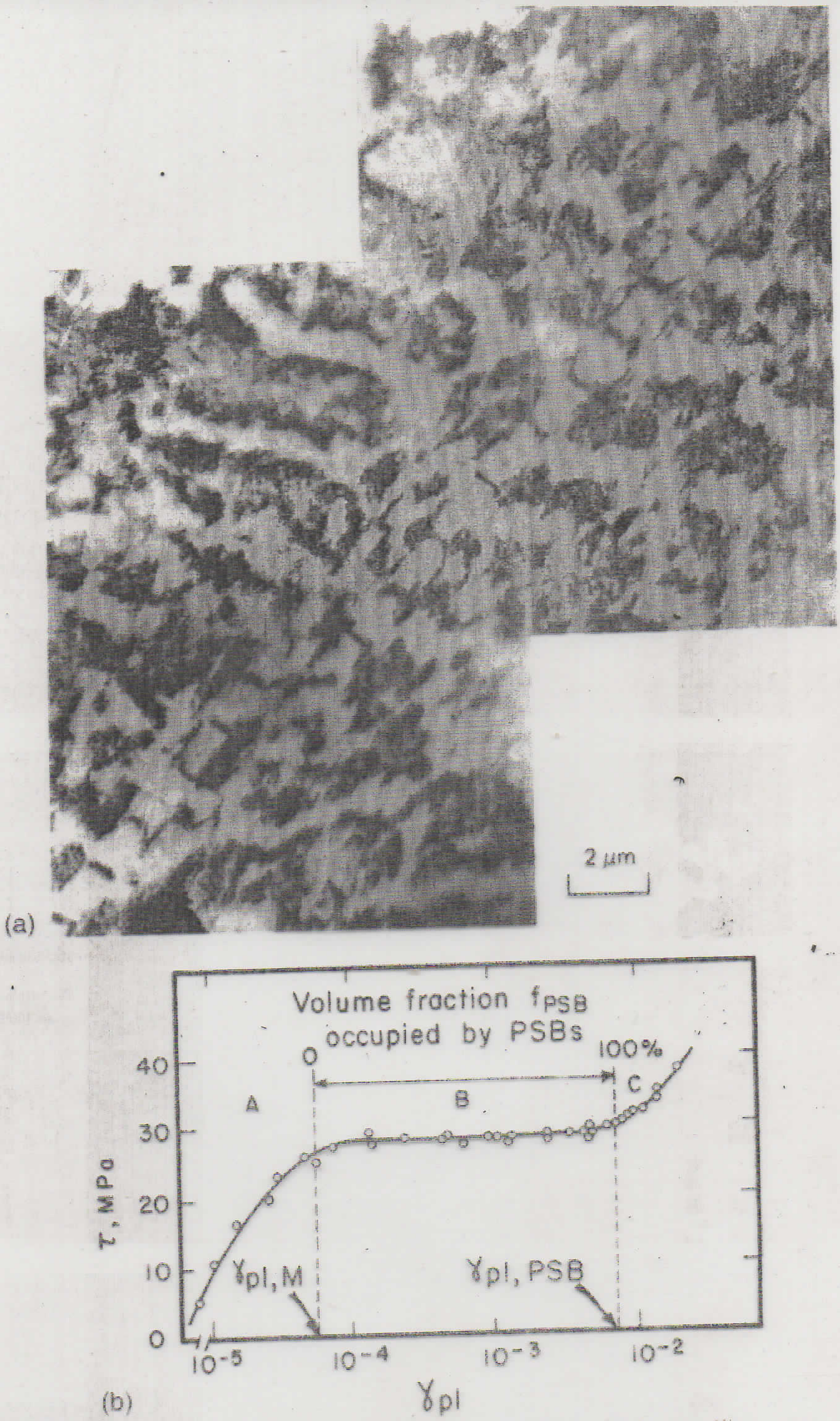

Figure 14.10 (a) Persistent slip bands in vein structure. Polycrystalline copper fatigued at a total strain amplitude of 6.4×10^{-4} for 3×10^5 cycles. Fatiguing carried out in reverse bending at room temperature and at a frequency of 17 Hz. The thin foil was taken 73 μm below the surface. (Courtesy of J. R. Weertman and H. Shirai) (b) Cyclic stress–strain curve for a single crystal of copper oriented for single slip (After H. Mughrabi, *Mater. Sci. & Eng.*, 33 (1978) 207.)

Figure 14.13 SEM of extrusions and intrusions in a copper sheet. (Courtesy of M. Judelwicz and B. Ilschner)

(a)

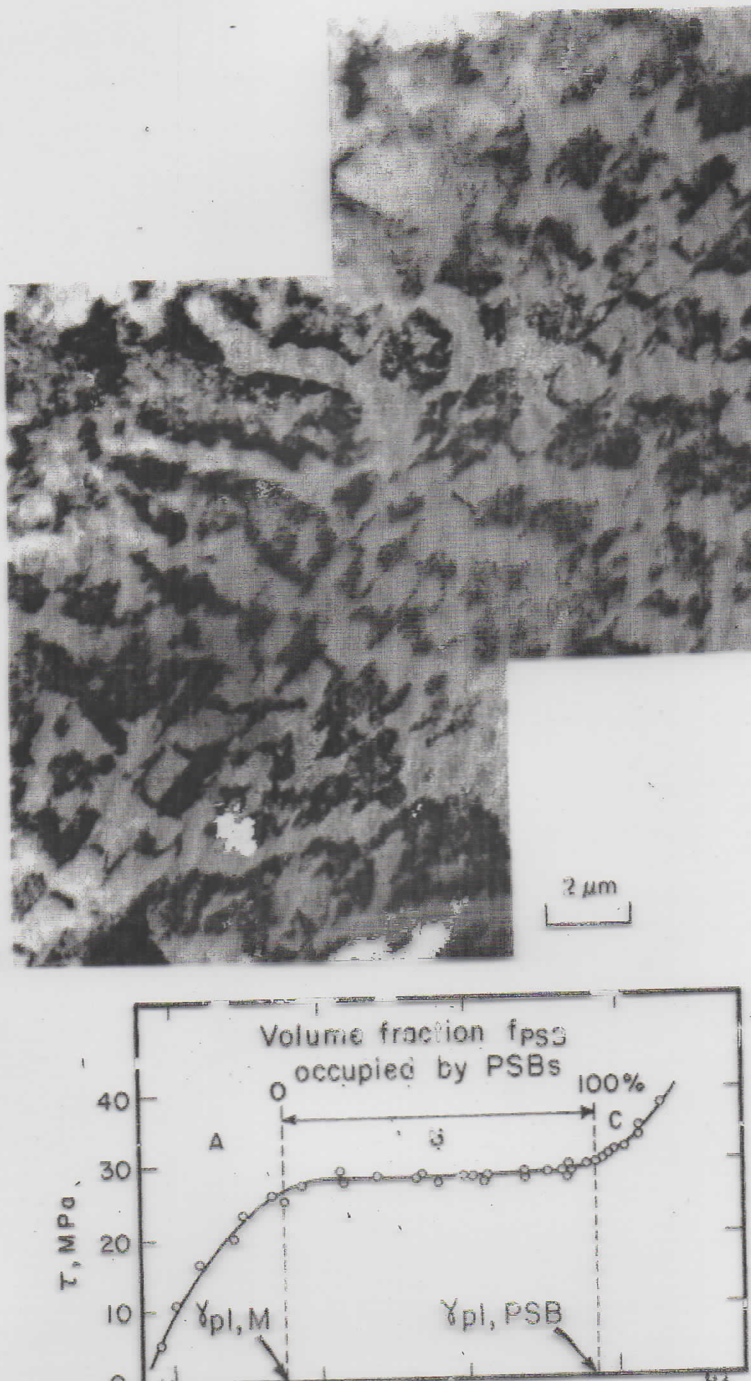

(b)

Figure 14.10 (a) Persistent slip bands in vein structure. Polycrystalline copper fatigued at a total strain amplitude of 6.4×10^{-4} for 3×10^5 cycles. Fatiguing carried out in reverse bending at room temperature and at a frequency of 17 Hz. The thin foil was taken 73 μm below the surface. (Courtesy of J. R. Weertman and H. Shirai) (b) Cyclic stress–strain curve for a single crystal of copper oriented for single slip (After H. Mughrabi, *Mater. Sci. & Eng.*, 33 (1978) 207)

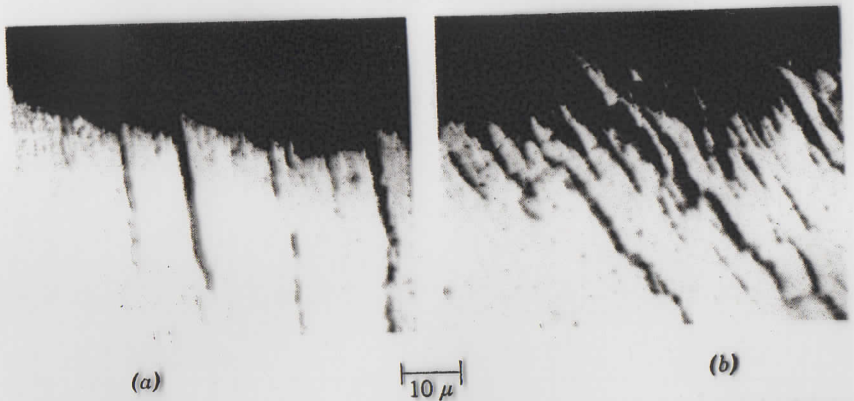

(a) (b)

Fig. 8. Taper sections from crystal 61: (a) Block movement; (b) fragmented primary-plane cracking. Taper magnification, 10X.

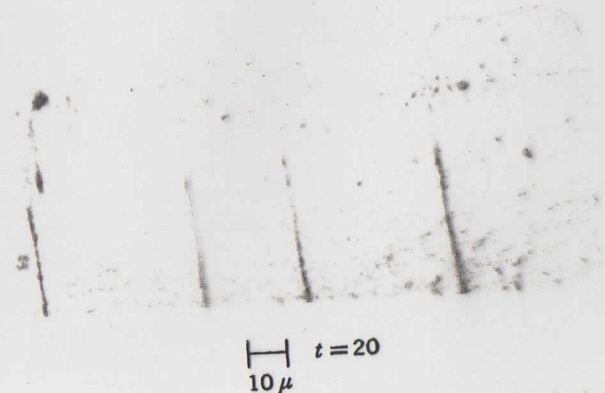

Fig. 14. Copper after $\frac{1}{10}$ of life. Slip bands developing surface notches.

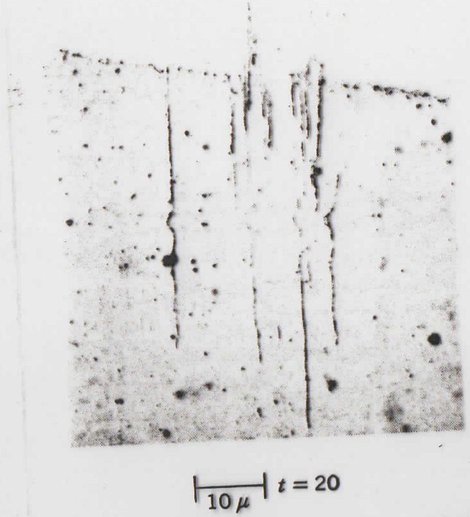

Fig. 15. Slip bands developing typical peak.

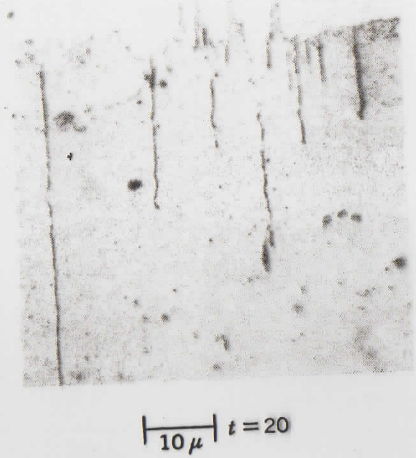

Fig. 16. Intermediate contours.

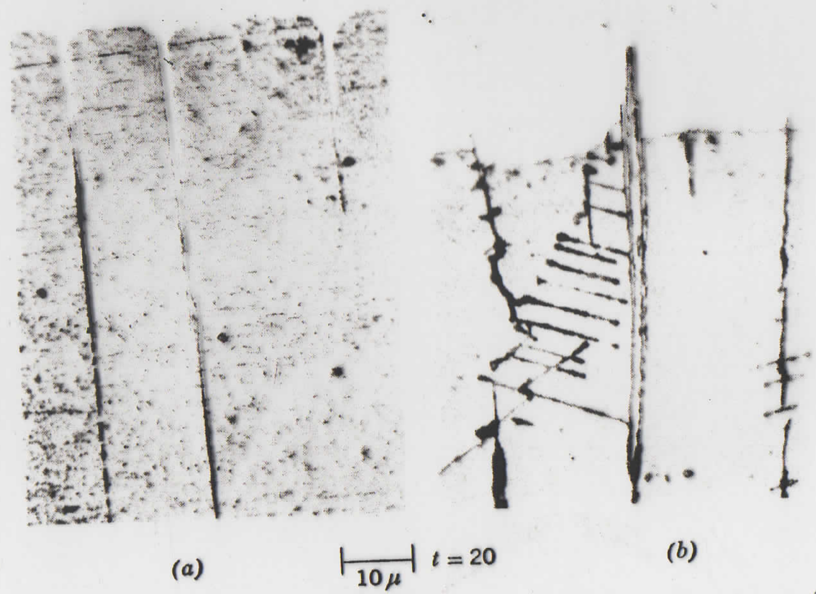

(a) (b)

Fig. 17. Copper at $\frac{1}{10}$ of life: (a) notches penetrating slip trace to form fissures, (b) fissures formed down each side of slip-band peak.

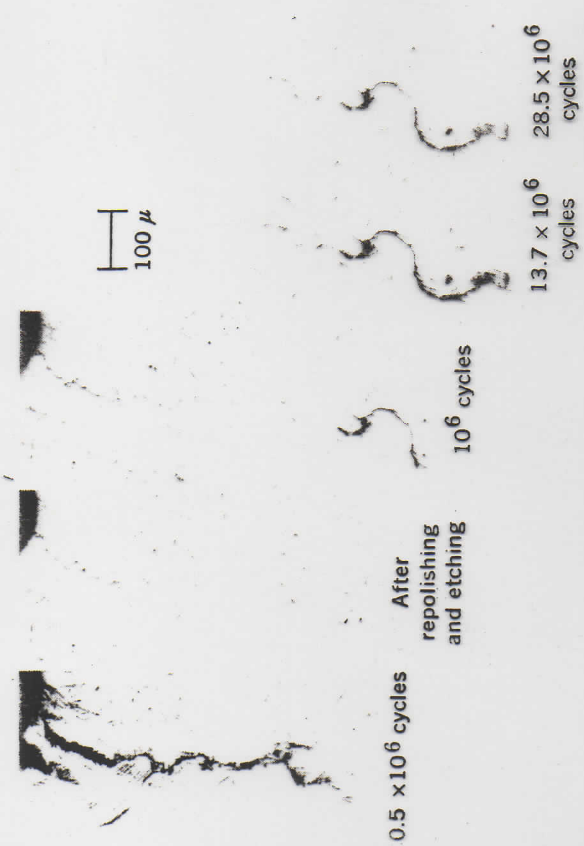

Fig. 7. Propagation of slip bands and cracks on notched specimen, 0.09% C steel. V-shaped notch.

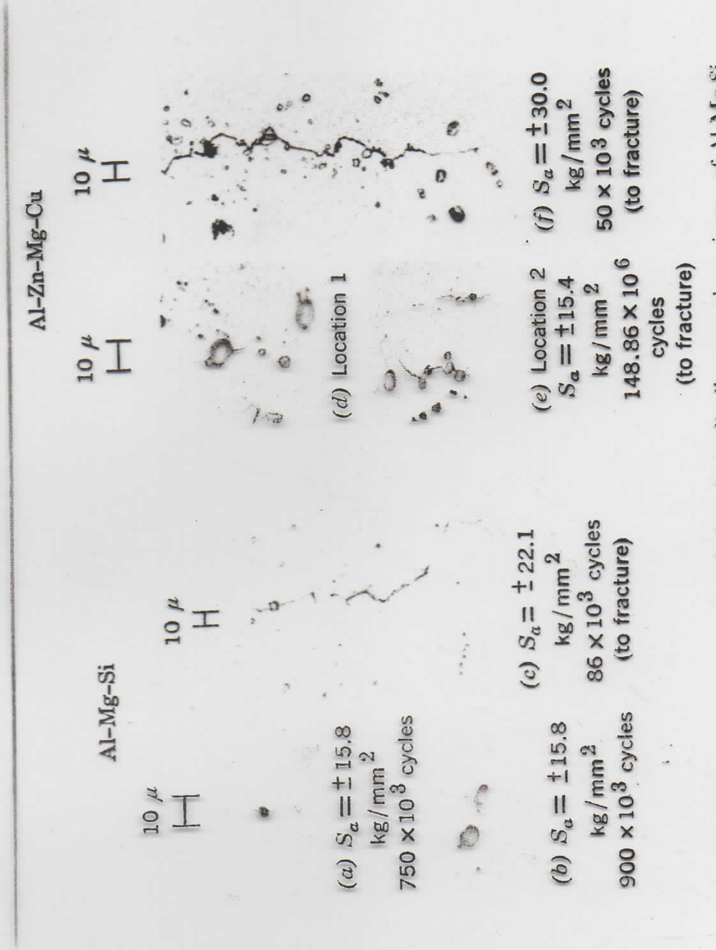

Fig. 24. Starting of cracks on inclusions in cyclically stressed specimens of Al-Mg-Si and Al-Zn-Mg-Cu alloys.

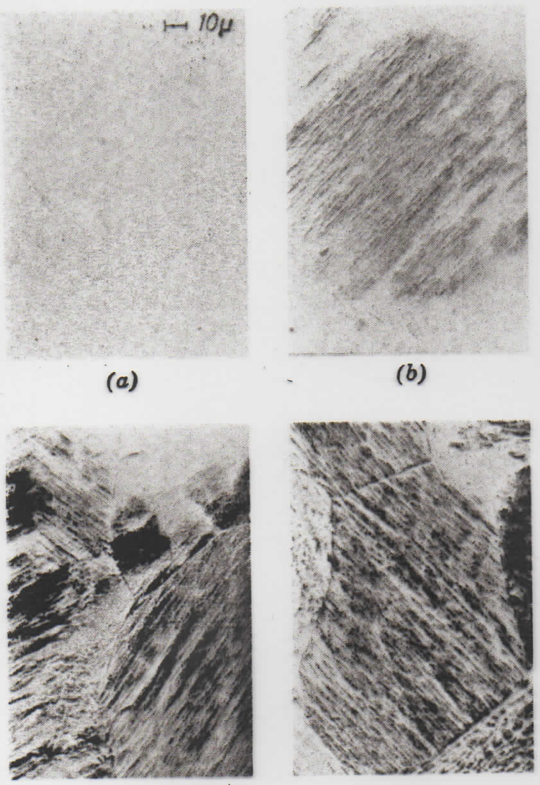

Fig. 16. Effect of increasing stress level on the appearance of slip markings in pure aluminum at a constant number of cycles, 0.25×10^6. S_a = (*a*) ± 0.73 kg/mm², (*b*) ± 0.93 kg/mm², (*c*) ± 1.34 kg/mm², (*d*) ± 1.74 kg/mm².

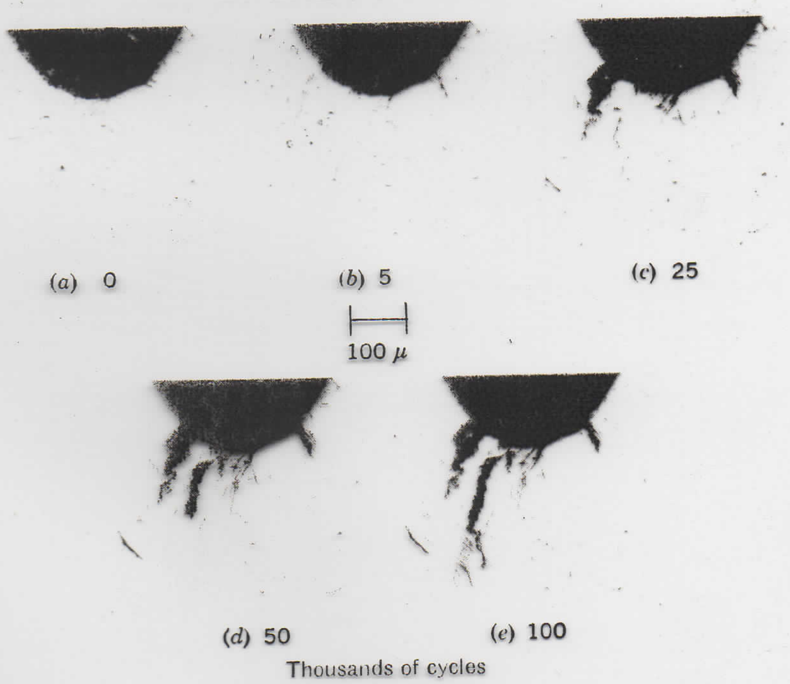

Fig. 5. Slip bands on 0.09% C steel specimen with V-shaped notch. $S_a = \pm 14.0$ kg/mm².

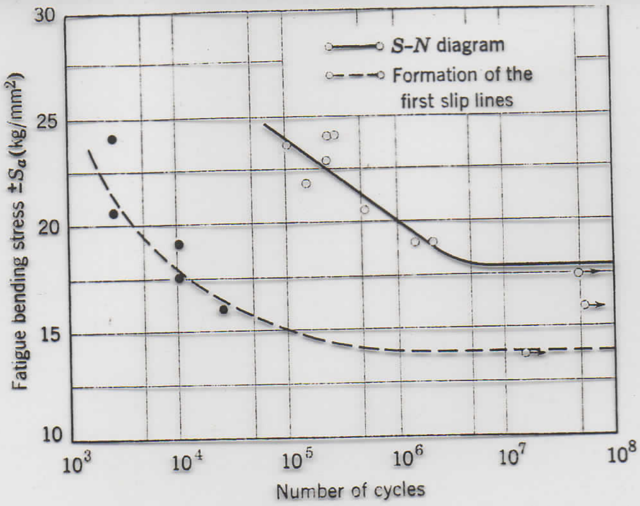

Fig. 3. Occurrence of the first slip lines on unnotched flat specimens of 0.09% C steel.

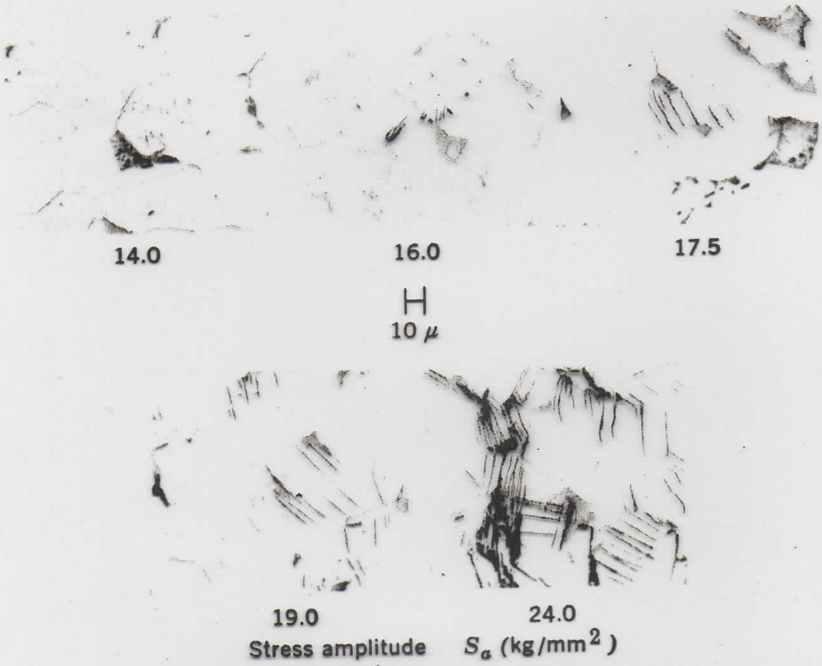

Fig. 4. Formation of slip bands dependent on the stress $\pm S_a$. 0.25×10^6 cycles.

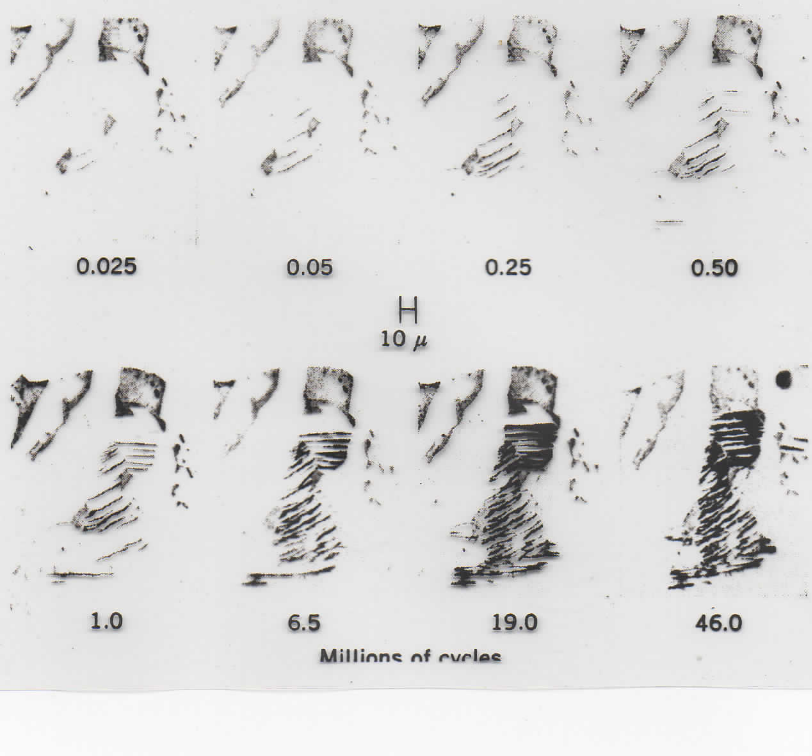

TABLE 17·1 Types of Loading*

LOAD		STRESS DISTRIBUTION	EXAMPLES
Axial	Tension		tensile test bars cables
	Compression		short columns
Bending	Simple	compression Neutral axis tension	Beams
	Cantilever	tension Neutral axis compression	Root of gear teeth
Torsional		Neutral axis shear	shafts coil springs
Direct shear		shear	rivets bolts
Contact		varies with depth and force direction	roller bearings gear teeth

*From D. J. Wulpi, "How Components Fail," American Society for Metals, Metals Park, Ohio, 1966.

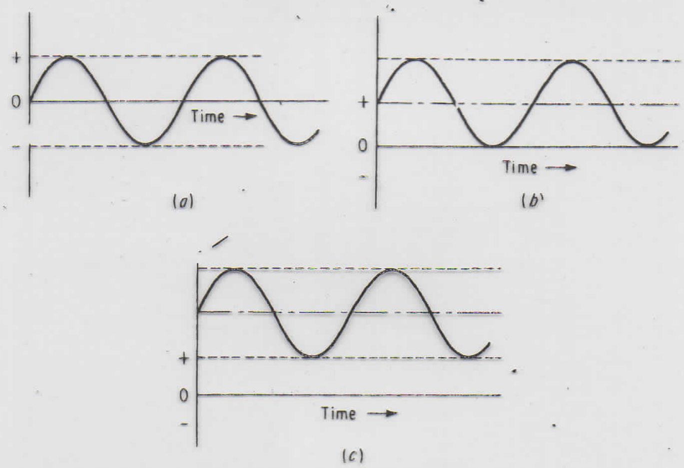

Fig. 17·7 The basic fatigue stress conditions. (*a*) Reversed stress, (*b*) unidirectional stress, (*c*) unidirectional stress with a preload.

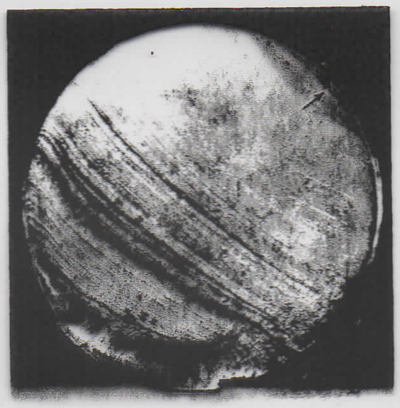

Fig. 17·8 The presence of "beach marks" usually indicates that failure was caused by fatigue. Here fracture began at a discontinuity (arrow). (Courtesy of D. J. Wulpi, International Harvester Company.)

TABLE 17-2 Residual Stresses Caused by Manufacturing Operations*

TENSILE STRESSES	COMPRESSIVE STRESSES	EITHER
Welding	Nitriding	Carburizing
Grinding	Shot peening	Rolling
Straightening	Flame and induction hardening	Casting
	Heat and quenching	Abrasive metal cutting (tensile stresses most common)
	Single-phase materials	Nonabrasive metal cutting
		Heat and quenching materials that undergo phase transformation (tensile stresses most common)

*From "Machine Design," The Penton Publishing Co., Cleveland, Oct. 16, 1969.

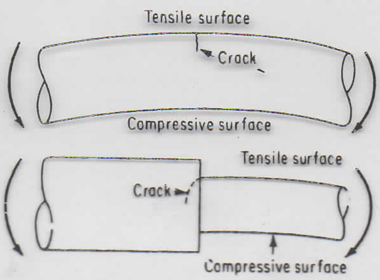

Fig. 17-28 Bending fractures usually develop on surfaces and normal to the stress direction. Sharp fillets concentrate bending stresses, causing cracks to develop more rapidly. Arrows indicate bending direction. (From D. J. Wulpi, "How Components Fail," American Society for Metals, Metals Park, Ohio, 1966.)

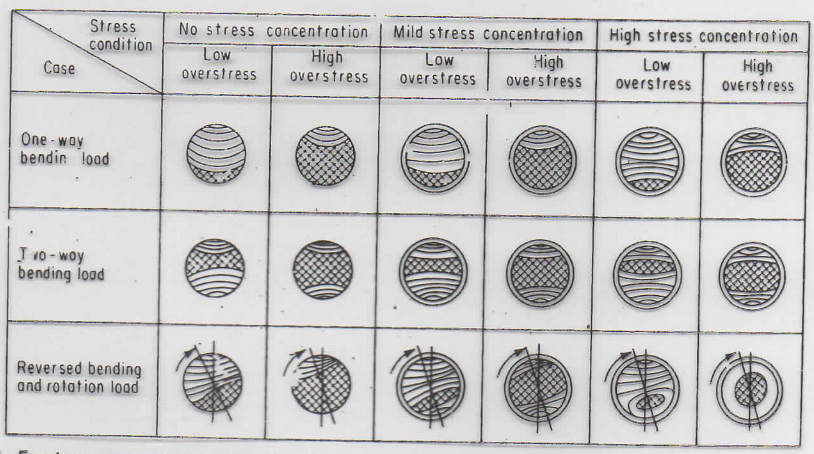

Fig. 17-27 Fracture appearances of bending-fatigue failures. Final fracture zones are shown as crosshatched areas. (From Machine Design, The Penton Publishing Co., Cleveland, Nov. 27, 1969.)

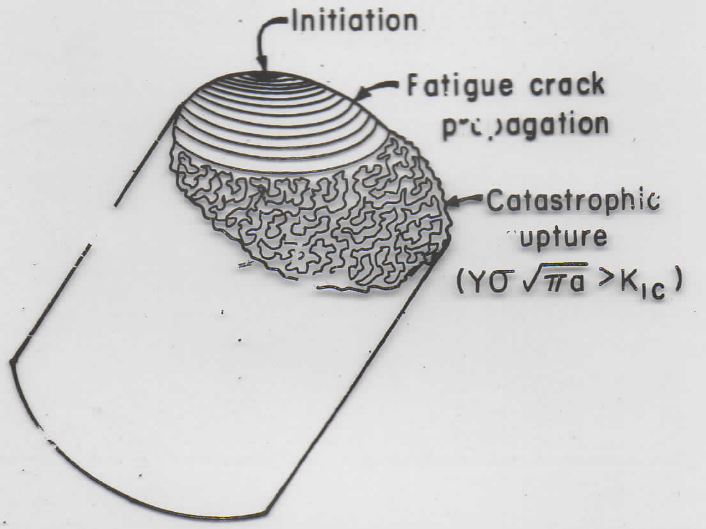

Figure 14.1 Schematic representation of a fatigue fracture surface in a steel shaft, showing the initiation region (usually at the surface), the propagation of fatigue crack (evidenced by beach markings), and catastrophic rupture when the crack length exceeds a critical value at the applied stress.

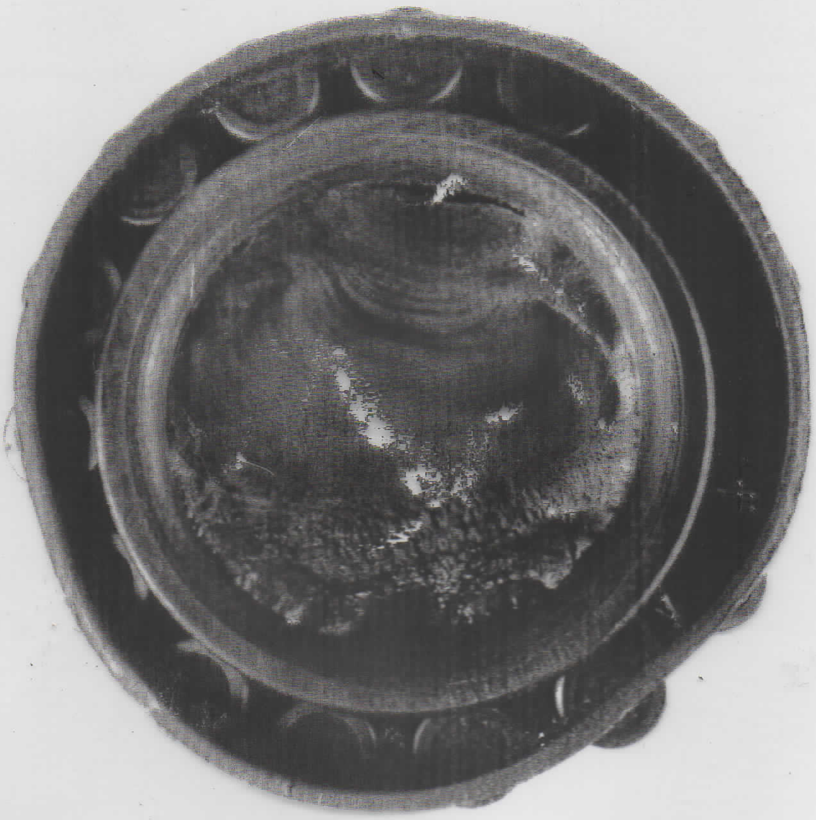

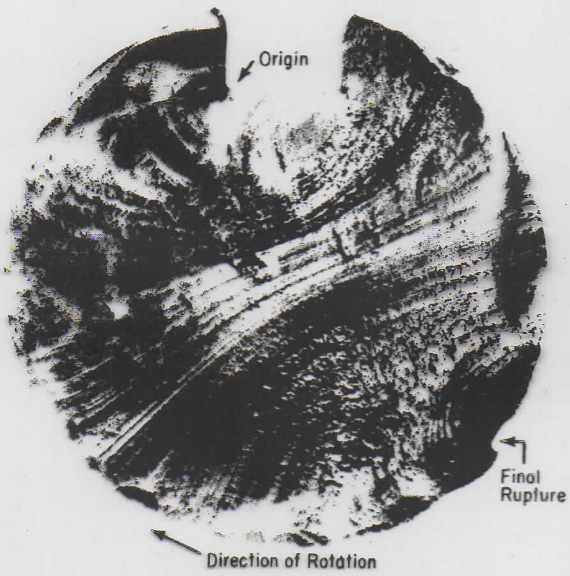

Fig. 17·12 The offsetting effect of rotation on the zone of final fracture reveals the direction that the shaft rotated during operation. (Courtesy of D. J. Wulpi, International Harvester Company.)

Fig. 17·10 "Ratchet marks" around edges of fatigue failures indicate that fracture began at several points. (Courtesy of D. J. Wulpi, International Harvester Company.)

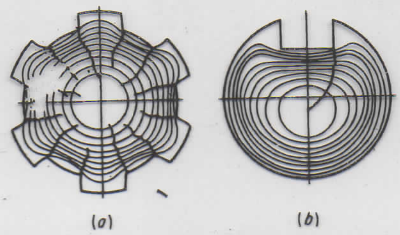

Fig. 17·17 Fatigue cracks tend to follow paths of maximum stress concentration. Circular lines indicate stresses. In splines and keyways, the stresses concentrate at inner corners. (*a*) Spline, (*b*) keyway. (From D. J. Wulpi, "How Components Fail," American Society for Metals, Metals Park, Ohio, 1966.)

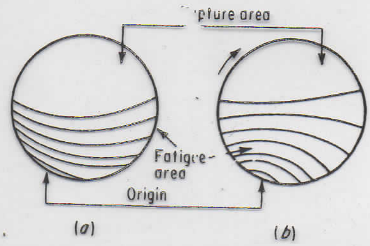

Fig. 17·16 The degree of notch sensitivity affects the manner in which beach marks develop. In notch-sensitive alloys, such as high-strength steel, these marks curve away from the source of failure (left). The reverse is true in notch-insensitive material (right). (From D. J. Wulpi, "How Components Fail," American Society for Metals, Metals Park, Ohio, 1966.)

Fig. 17·14 Sectional valve bonnet showing crack which originated at the sharply machined corner. (From R. D. Barer and B. F. Peters, "Why Metals Fail," Gordon and Breach Science Publishers, New York, 1970.)

Fig. 17·29 This 1050 shaft, 1.94 in. in diameter, broke in reversed bending fatigue. A sharp fillet concentrated the bending stresses, causing a crack to develop on opposite sides with final fracture in the middle. (Courtesy of D. J. Wulpi, International Harvester Company.)

Fig. 17·30 Some rotating bending-fatigue failures begin beneath surfaces. In this induction-hardened axle shaft, fracture started at *A* and moved into the cross section, meeting another subsurface crack that started at *B*, resulting in final fracture. (Courtesy of D. J. Wulpi, International Harvester Company.)

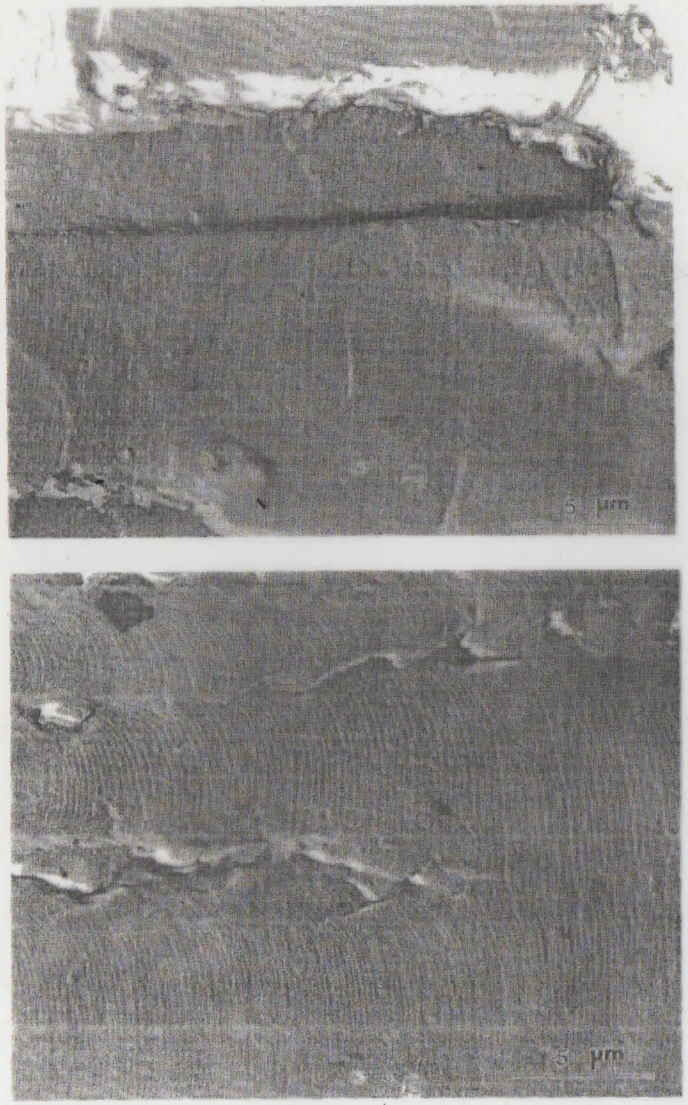

Figure 14.17 Fatigue striations in 2014-T6 aluminum alloy; two-stage carbon replica viewed in TEM. (a) Early stage. (b) Late stage. (Courtesy of J. Lankford)

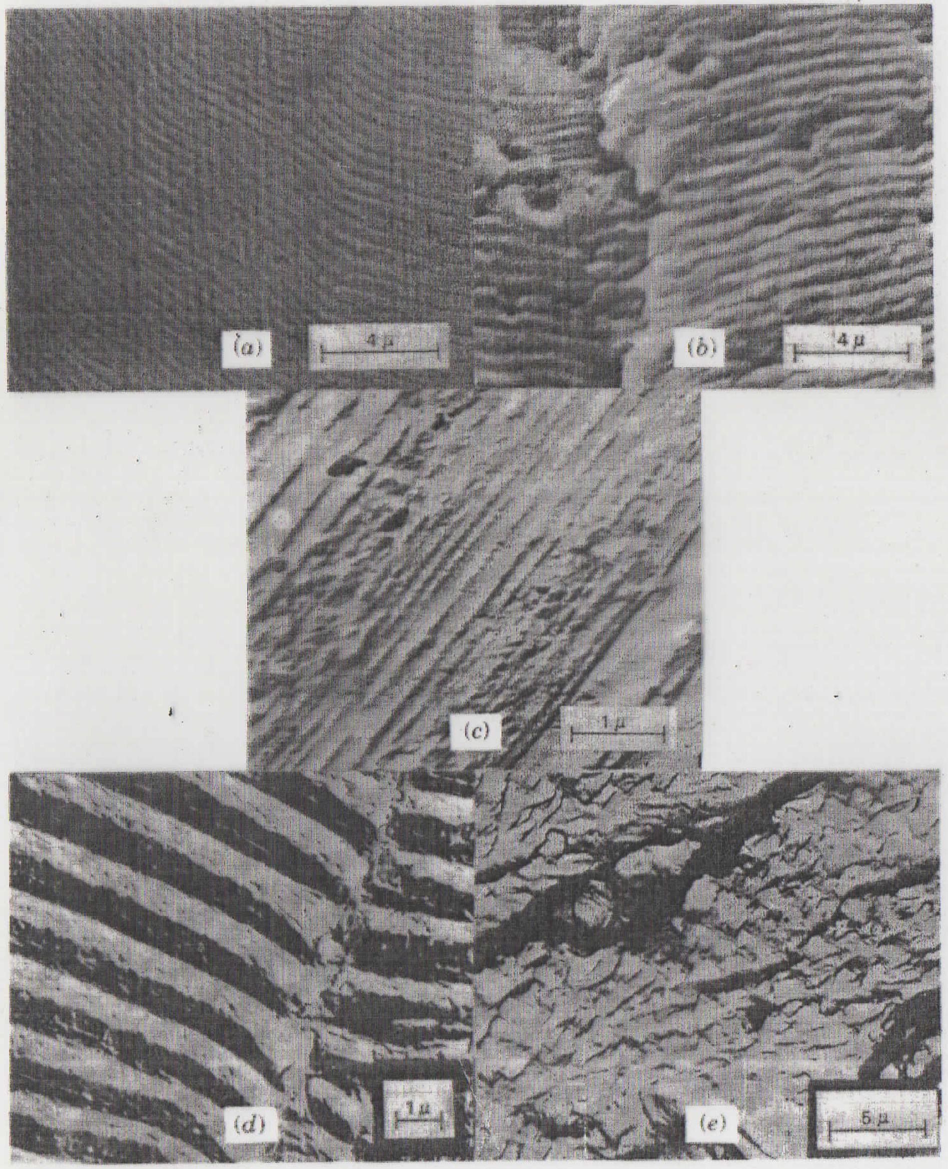

FIGURE 13.11 **Electron fractographs revealing fatigue striations found on fracture surface and within macroscopic bands (Figs. 12.1, 12.3, 13.42). (*a*) TEM, constant load range; (*b*) SEM, constant load range; (*c*) TEM, random loading; (*d*) TEM, ductile striations.[22]; (*e*) TEM, brittle striations.[22] (Reprinted with permission of the American Society for Testing and Materials from copyrighted work.)**

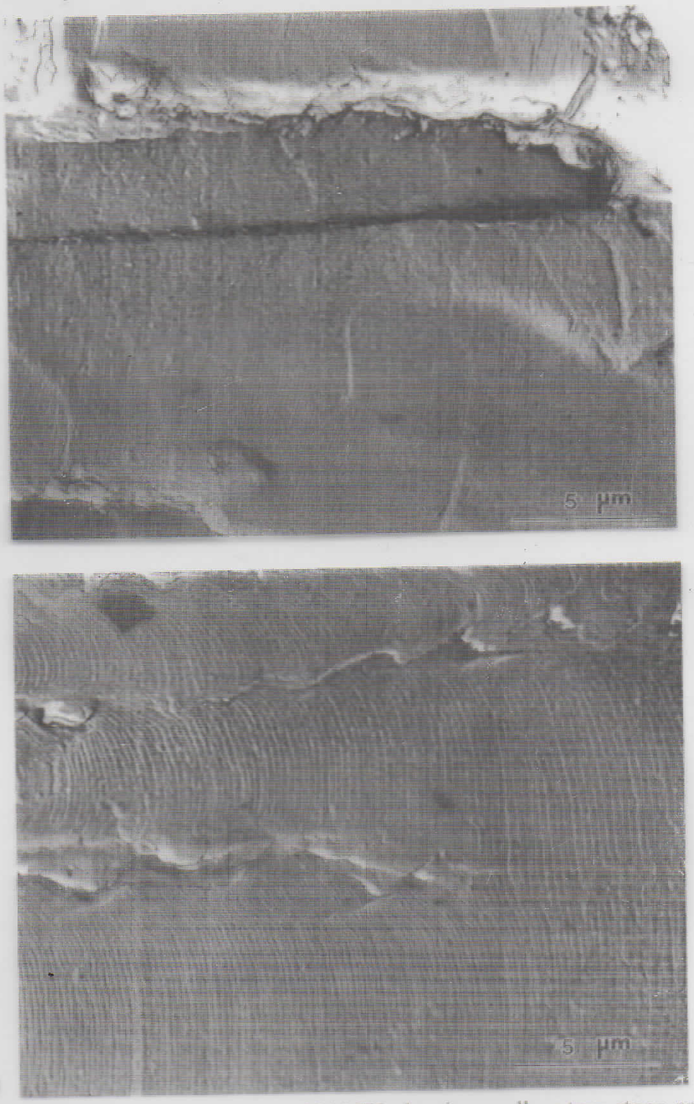

(a)

(b)

Figure 14.17 Fatigue striations in 2014-T6 aluminum alloy; two-stage carbon replica viewed in TEM. (a) Early stage. (b) Late stage. (Courtesy of J. Lankford)

10 μ

Fig. 14. Microfractograph of a fatigue rupture surface of mild steel (rupture in 0.64×10^6 cycles under 12 ± 19 kg/mm² direct stress).

10 μ

Fig. 15. Microfractograph of a fatigue rupture surface of duralumin (alternate bending, ± 7 kg/mm², rupture in 0.27×10^6 cycles).

10 μ

Fig. 16. Microfractograph of a fatigue rupture surface of 18-8 stainless steel (direct stress, ± 23 kg/mm², rupture in 77,000 cycles).

10 μ

Fig. 17. Microfractograph of a fatigue rupture surface of 18-8 stainless steel (rotating bending, ± 24 kg/mm², rupture in 0.87×10^6 cycles).

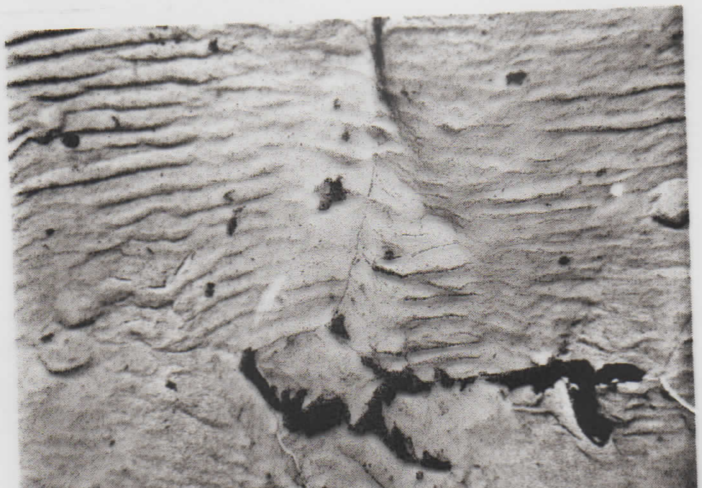

10 μ

Fig. 18. Microfractograph of a fatigue rupture surface of mild steel